

This document is the unedited Author's version of a Submitted Work that was subsequently accepted for publication in Langmuir, copyright © American Chemical Society after peer review. To access the final edited and published work see <https://pubs.acs.org/doi/10.1021/acs.langmuir.8b02402> . Access to this work was provided by the University of Maryland, Baltimore County (UMBC) ScholarWorks@UMBC digital repository on the Maryland Shared Open Access (MD-SOAR) platform.

Please provide feedback

Please support the ScholarWorks@UMBC repository by emailing scholarworks-group@umbc.edu and telling us what having access to this work means to you and why it's important to you. Thank you.



Published in final edited form as:

Langmuir. 2018 November 20; 34(46): 13924–13934. doi:10.1021/acs.langmuir.8b02402.

Synthesis and Degradation of Cadmium-Free InP and InPZn/ZnS Quantum Dots in Solution

Richard P. Brown[†], Miranda J. Gallagher[‡], D. Howard Fairbrother[‡], and Zeev Rosenzweig^{*,†}

[†]Department of Chemistry and Biochemistry, University of Maryland Baltimore County, Baltimore, Maryland 21250, United States

[‡]Department of Chemistry, Johns Hopkins University, Baltimore, Maryland 21218, United States

Abstract

This study advances the chemical research community toward the goal of replacing toxic cadmium-containing quantum dots (QDs) with environmentally benign InP QDs. The InP QD synthesis uniquely combines the previously reported use of InP magic-sized clusters (MSCs) as a single-source precursor for indium and phosphorus to form InP QDs, with zinc incorporation and subsequent ZnS shelling, to form InPZn/ZnS QDs with luminescence properties comparable to those of commonly used cadmium-containing luminescent QDs. The resulting InPZn/ZnS QDs have an emission quantum yield of about 50% across a broad range of emission peak wavelengths and emission peaks averaging 50 nm fwhm. The emission peak wavelength can be easily tuned by varying the Zn/In ratio in the reaction mixture. The strategy of using zinc stearate to tune the emission properties is advantageous as it does not lead to a loss of emission quantum yield or emission peak broadening. Although the initial optical properties of InP and InPZn/ZnS QDs are promising, thermal stability measurements of InPZn QDs show significant degradation in the absence of a shell compared to the CdSe QDs particularly at increased temperature in the presence of oxygen, which is indicative of thermal oxidation. There is no significant difference in the degradation rate of InP QDs made from molecular precursors and from MSCs. Additionally, the emission intensity and quantum yield of InPZn/ZnS QDs when purified and diluted in organic solvents under ambient conditions decrease significantly compared to those of CdSe/ZnS QDs. This indicates instability of the ZnS shell when prepared by common literature methods. This must be improved to realize high-quality, robust Cd-free QDs with the capability of replacing CdSe QDs in QD technologies.

Graphical Abstract

*Corresponding Author zrosenzw@umbc.edu.

Notes

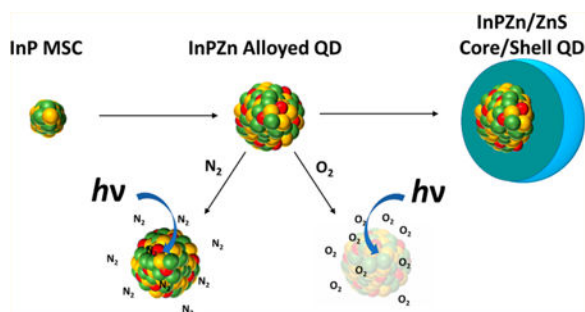
The authors declare no competing financial interest.

ASSOCIATED CONTENT

Supporting Information

The Supporting Information is available free of charge on the ACS Publications website at DOI: [10.1021/acs.langmuir.8b02402](https://doi.org/10.1021/acs.langmuir.8b02402).

HRTEM of InPZn quantum dots (Figure S1), calculation of extinction coefficient for InP(MA) MSCs, plot of peak energy for different Zn/In ratios (Figure S2) (PDF)



INTRODUCTION

InP/ZnS and InPZnS/ZnS core/shell and alloy/shell quantum dots (QDs) have been recently proposed as a viable, cadmium-free alternative to cadmium-containing QDs, such as CdS/ZnS, CdSe/ZnS, and CdTe/CdSe/ZnS QDs.^{1–5} Historically, a major challenge for InP QD synthesis lies in the need to replace highly reactive, pyrophoric phosphorus precursors such as tris(trimethylsilyl)phosphine [P(TMS)₃] with safer and more stable precursors. In addition to posing significant safety concerns, the use of highly reactive molecular precursors leads to heterogeneous crystal growth, broad InP QD size distribution, and broad emission peaks.⁶ Another challenge lies with the inherently low photoluminescence (PL) quantum yield of InP QDs. The low quantum yield of about 1% has been attributed to nonradiative exciton relaxation pathways associated with unsaturated “dangling” phosphorus bonds.⁷ One approach to increase the photoluminescence quantum yield involves coating the InP QD cores with a higher energy band gap material such as ZnS.⁸ The ZnS shell passivates surface defects, confines excitons, prevents core oxidation, and significantly increases the photoluminescence quantum yield of InP/ZnS core/shell QDs to about 40%.^{9,10} Another approach has been to grow an interfacial layer between the core and the shell to better passivate defects and to enable the formation of a more complete shell. This approach was reported to increase the photoluminescence quantum yield of InPZnS/ZnS QD up to 70%. However, the photoluminescence quantum yield of QDs that were prepared using this technique varied greatly with emission wavelength. The resulting QDs were heterogeneous in size, which resulted in broad emission peaks.⁴ Other studies have attempted to narrow the size distribution of InP QDs by replacing the highly reactive phosphorus molecular precursors with less reactive molecular precursors such as tris(trimethyl)germanium phosphide, triarylsilylphosphine, and aminophosphine.^{11–13} This resulted in some narrowing of the size distribution and emission peaks but did not lead to significant improvement in the photoluminescence quantum yield of InP/ZnS QDs. Furthermore, most strategies for tuning the optical properties result in inconsistent QD properties and a need to optimize many reaction parameters. Table 1 summarizes how fwhm values can change depending on emission color.^{1,4,14,15} Recently, Lee and co-workers published a technique for making InP-based core/shell QDs with peaks less than 40 nm fwhm.¹⁵ Their results are quite impressive but rely on a much longer reaction time of around 5 h and a complicated setup, which highlight the need for simple, highly reproducible methods for making high-quality InP-based QDs. Studies by Cossairt and co-workers demonstrated the possibility of forming monodisperse InP QDs using magic-sized clusters (MSCs) as the source of both phosphorus

and indium.⁶ MSCs are obtained in a wide range of nanocrystals, and their presence plays a significant role in many crystal growth mechanisms.^{16–18} Cossairt and co-workers discovered that InP MSCs could be synthesized in gram quantities from $P(TMS)_3$ and indium myristate (MA) at a relatively low temperature and used as a single-source precursor for the synthesis of InP QDs.⁶ They also obtained the crystal structure of phenyl acetate (PA)-coated InP MSCs using X-ray crystallography, allowing them to determine the core structure and atomic formula of InP MSCs to be $In_{37}P_{20}$.¹⁹

In this paper, we demonstrate a simple and scalable synthesis method to form highly luminescent InPZn/ZnS QDs from nonpyrophoric InP(MA) MSCs and zinc stearate. Including zinc stearate in the reaction mixture provides an easy and reproducible method for controlling the size and band gap of the resulting QDs. Coating these InPZn QDs with a ZnS shell is performed without any purification steps to produce strongly luminescent core/shell InPZn/ZnS QDs with high photoluminescence quantum yield and decently narrow and tunable emission peaks. Unique to this strategy is the maintenance of high photoluminescence quantum yield and emission peak width over a broad range of emission wavelengths. Although these numbers are not “record breaking”, the simplicity and speed of this strategy provide significant value to the field. Additionally, this synthesis approach eliminates the use of pyrophoric precursors in the high-temperature QD synthesis and leads to the formation of luminescent QDs with optical properties rivaling those of the widely used CdSe/ZnS QDs. Employing InP MSCs as a single source reactant for indium and phosphorus in the synthesis of luminescent InPZn/ZnS QDs alleviates significant safety concerns because the exposure to $P(TMS)_3$ is minimized to a single, low-temperature procedure used to form the InP MSCs in high yield. The resulting InP MSCs are nonpyrophoric and could be used to synthesize >100 samples of highly luminescent InPZn/ZnS QDs in milligram quantities from the same batch of InP MSCs. The use of InP MSCs as a precursor leads to improved consistency and reproducibility of the InPZn/ZnS QD structure and properties by greatly simplifying their synthesis (Scheme 1). This study also evaluates the chemical and thermal stability of InPZn QDs that are made from InP MSCs and compares them to InP and CdSe QDs made from molecular precursors. Long-term chemical and thermal stability of luminescent QDs is imperative to the functionality of QD-based consumer electronic devices, which often operate at increased temperatures. Methods to improve stability often rely on thick silica coatings²⁰ or embedding the QD into polymers.²¹ These strategies, however, do not apply to small colloidal QDs that are intended for biological imaging and sensing applications. A limited number of studies have been conducted to evaluate the chemical and thermal stability of colloidal InP QDs toward photoinduced or thermally induced oxidation.^{22,23} Typically, these experiments monitor core/shell QD photoluminescence over time under constant illumination. More insight can be gained, however, by studies such as those performed by Houtepen and co-workers who evaluated various InP-based QDs alloyed with Ga and Zn under constant illumination and showed that certain multishell configurations provide superior stability.²⁴ In a different study, Zhang and co-workers showed that InPZn QDs made from PH_3 (P precursor) and zinc stearate increased in photoluminescence, and their absorption spectrum remained stable for over 30 days when the QDs were suspended in hexane and stored in the dark.²⁵ They attributed the photoluminescence enhancement to oxidation of P, which resulted in the

elimination of dangling phosphorus bonds. The limited number of studies did not look systematically at the effects of heat and oxygen on core degradation.

MATERIALS AND METHODS

Reagents.

Tris(trimethylsilyl)phosphine, $\text{P}(\text{TMS})_3$ (98%), was purchased from Strem Chemicals, and hexamethyldisilathiane, $\text{S}(\text{TMS})_2$ (synthesis grade), was purchased from Sigma-Aldrich. Both were handled in a nitrogen-filled glovebox. Zinc formate (98%) and 1-dodecylphosphonic acid (95%) were purchased from VWR. All other chemicals were purchased from Sigma-Aldrich. Indium(III) acetate (99.99% trace metal basis), myristic acid (99%), zinc stearate (purum grade), cadmium acetylacetonate (99.9% trace metals basis), tetradecylphosphonic acid (97%), hexadecylamine (98%), and oleylamine (98%) were used as received. Anhydrous trioctylphosphine (97%) was stored in the glovebox. 1-Dodecanethiol and oleic acid (90%) were degassed and stored in the glovebox. Squalane (96%) and 1-octadecene (90%) were dried over CaH_2 , distilled, and stored over molecular sieves in the glovebox. Toluene (99.8%), pentane (99%), and acetonitrile (99.8%) that were used for synthesis were all anhydrous grade and stored over molecular sieves in the glovebox. All air-sensitive manipulations were performed under inert conditions, either in a glovebox or on a Schlenk line in the fume hood. The Schlenk line was supplied by high-purity N_2 which passed through a cylinder filled with drierite. Solvents used for the degradation studies were ACS grade and used without further purification.

Extreme caution should be taken when working with $\text{P}(\text{TMS})_3$. It is pyrophoric when exposed to air, and phosphides, in general, can form PH_3 , an extremely toxic gas when exposed to acidic protons, including water. Small quantities of $\text{P}(\text{TMS})_3$ residue should be carefully quenched with bleach in a well-ventilated fume hood.

Synthesis of Myristate-Coated InP Magic-Sized Clusters (InP(MA) MSCs).

InP(MA) MSCs were made according to a scaled-up version of Cossart's method.⁶ We typically used the entire ampule of $\text{P}(\text{TMS})_3$ from the chemical supplier so as to not leave unused pyrophoric reagents in the lab. As heterogeneous thermal mixing is less of a concern with equilibrium reactions, we anticipate that this reaction could be scaled to much larger industrial-sized productions. The reaction was carried out in a three-neck flask, which was equipped with a thermocouple, condenser, septum, and stir bar. (The following amounts should be adjusted after determining the exact amount of $\text{P}(\text{TMS})_3$ in the supplied ampule.) A typical flask contained indium acetate (9.5 mmol) and myristic acid (34.4 mmol). The reaction mixture was then degassed (vac/fill multiple times) and heated under nitrogen until all reactants were melted and well mixed. Vacuum was carefully applied, trying to avoid splattering while heating to 100 °C. The mixture was left overnight under vacuum at 100 °C to form indium myristate. The next day, the system was backfilled with N_2 , and dry toluene (40 mL) was added to the indium myristate and heated to 110 °C. $\text{P}(\text{TMS})_3$ (4 mmol) was dispersed in dry toluene (20 mL) in a syringe equipped with a needle in the glovebox. After being capped with a septum, the syringe was transferred to the fume hood and added to the In(MA) mixture. The reaction was monitored by taking samples for UV-vis absorption

spectroscopy measurements at various time intervals. Almost immediately, the color changed from clear to yellow. After about 45–60 min, the excitonic peak was fully defined and no longer changed, showing evidence of reaching completion. After cooling, toluene was removed by applying vacuum in the Schlenk line, and the crude product was transferred to the glovebox for purification while carefully avoiding the introduction of air. Cooling the toluene on ice and carefully using a room temperature water bath to alternate warming/cooling made evaporation much easier to control on the high-vacuum levels of our Schlenk line. In the glovebox, small portions of dry toluene were used to transfer and dissolve the crude MSCs to airtight centrifuge tubes. The sealed tubes were removed from the glovebox for centrifugation. After each centrifugation, the tubes were returned to the glovebox for all manipulations. An initial centrifugation (10000g, 15 min) was used to remove insoluble material, and supernatant was transferred to a clean centrifuge tube to be precipitated with dry acetonitrile. After 3–5 precipitation/centrifugation/resuspension washes (10000g, 5 min) with dry toluene and dry acetonitrile under N₂, dry pentane was used to dissolve and transfer the final MSC pellet to a clean scintillation vial. Careful evaporation of the pentane yielded pure InP(MA) MSCs as a waxy bright yellow solid. Later dissolution into room temperature squalane produced a completely translucent yellow solution. If MSCs were carefully protected from air during the washing procedure, the UV–vis absorption spectrum remained unchanged after the washing procedure.

Synthesis of InPZn Alloyed Core Quantum Dots from Magic-Sized Clusters (InPZn MSC QD Core) (Scheme 1).

A typical synthesis to form InPZn (25% Zn/In) MSC QD cores is as follows. A three-neck round-bottom flask equipped with a thermocouple, condenser, and glass-coated stir bar was attached to the Schlenk line. Sixty-six micromoles of zinc stearate and 7.5 mL of dry squalane were added, and the flask was plugged with a rubber septum. With stirring, the flask was evacuated and filled with nitrogen multiple times and heated under vacuum until the squalane almost began to boil, whereupon the flask was filled with nitrogen and the TC was set to around 200 °C. Meanwhile, a syringe of 100 mg of InP MSCs in 2 mL of dry squalane was prepared in a glovebox and capped with a septum to allow for transfer outside the glovebox. When everything was ready, the TC was set to a very high temperature (around 600 °C) to allow for rapid heating. The InP MSC solution was swiftly injected into the hot zinc stearate solution when the temperature reached greater than 395 °C. Because of the room temperature injection, the reaction temperature would decrease to around 360 °C and increase to about 370 °C in about 1 min. At 1 min, the mantle was removed, and the extremely hot flask was carefully lowered into a room temperature silicone oil bath to cool quickly. A portion could be removed and stored in the glovebox as InPZn MSC QD cores for future analysis.

Synthesis of InPZn/ZnS MSC Core/Shell QDs.

Once at room temperature, an additional 200 μ mol of zinc stearate was added to the above reaction mixture under nitrogen flow. The mixture was degassed multiple times and heated to 230 °C under N₂. After 3 h and without cooling, 200 μ L of 1 M 1-dodecanethiol in dry squalane was added over 15 min by a syringe pump. After 1 h at 230 °C to allow for ZnS shell to grow, the reaction mixture was cooled, transferred to a 20 mL glass scintillation vial,

and flushed with nitrogen before storing. Core/shell QDs are significantly more resistant to water/oxygen degradation than InP MSCs or even InP QD cores. The core/shell QDs can be handled easily on the benchtop using standard solvents. Although any effort to exclude light and oxygen will help maintain their desired properties, extreme measures are not necessary. Storing at room temperature in the dark maintains sufficiently bright QDs, but immediate transfer to the glovebox appeared to maintain higher luminescence stability when InPZn/ZnS QD solutions were stored for long periods. QD purification was realized by first diluting the InPZn/ZnS QDs in toluene and removing insoluble precipitates by centrifugation. We then added a small amount of ethyl acetate as a cosolvent (for the viscous squalane) and precipitated the QDs with acetonitrile. Initial precipitation by centrifugation yields an oily liquid pellet. Further washing cycles, which include resuspension in toluene, precipitation with acetonitrile, and centrifugation, yield compact QD pellets that disperse fully in nonpolar solvents.

Synthesis of InPZn/ZnS MSC QDs with Varying Emission Peak Wavelength.

The size and emission peak of InPZn/ZnS MSC QDs are affected by many parameters including InP MSC concentration, reaction temperature, and injection volume (which affects temperature decrease after injection). However, we found that increasing the concentration of zinc stearate, while keeping all other parameters constant, enables tuning the λ_{max} of the emission peak to the blue while maintaining narrow emission peak widths (fwhm). See Table 2 for suggested concentrations for targeting specific wavelengths. All concentrations are given as a percent zinc stearate to total indium; %50 means that 100 mg of InP(MA) MSCs = 225 μmol of indium, and therefore 112.5 μmol of zinc stearate should be used. The shelling procedure is identical for each size.

Synthesis of CdSe and CdSe/ZnS Core and Core/Shell QDs.

CdSe core and CdSe/ZnS core/shell QDs were made according to the method published by Mulvaney, with slight modifications.²⁶

CdSe Core QDs.

In a nitrogen-filled glovebox, selenium powder (4.2 mmol) was dissolved in trioctylphosphine (5 mL) by stirring in a vial for about 1 h. In a 50 mL three-neck flask, a magnetic stir bar, cadmium acetylacetonate (1.0 mmol), hexadecylamine (20.7 mmol), tetradecylphosphonic acid (2.1 mmol), and trioctylphosphine (10 mL) were combined, and the flask was equipped with a septum, thermocouple, and condenser. This mixture was degassed under multiple cycles of vacuum/purge on a nitrogen-filled Schlenk line. Then the solution was heated to 100 °C under vacuum for >30 min. After being backfilled with N₂, the solution was heated to 250 °C for 1 h to dissolve the cadmium precursor. The mixture was allowed to cool to 120–100 °C, and vacuum was reapplied for 30 min to remove any volatile side products. Finally, the reaction flask was filled with nitrogen and heated to 320 °C, where the mantle was set to 270 °C. When the temperature decreased to 300 °C, the TOP-Se solution from the glovebox was swiftly injected into the hot reaction mixture. The temperature decreased to 260 °C, and crystal growth occurred up to 270 °C for 5 min after injection, whereupon the reaction mixture was cooled quickly and allowed to anneal at 80 °C for 30 min.

CdSe/ZnS Core/Shell QDs.

A total of 6.5 mL of room temperature CdSe crude reaction mixture was mixed with butanol (4 mL), vortexed, and centrifuged (3000g for 5 min). The supernatant was discarded, and the pellet was resuspended in CHCl_3 (5 mL). The QDs were centrifuged again (3000g for 5 min). The QD layer was removed to a clean vial, and 4:1 acetone/methanol (about 5 mL) was added to precipitate the QDs. After a final centrifugation (3000g for 5 min), the QD pellet was resuspended in hexane (5 mL). UV-vis absorbance was used to determine concentration [$25 \mu\text{M}$] (4.8 mL) = $0.12 \mu\text{mol}$; $\epsilon_{532} = 172284 \text{ L mol}^{-1} \text{ cm}^{-1}$ was estimated using Mulvaney's equation relating excitonic peak position to QD size and molar extinction coefficient.²⁶ Zinc and sulfur precursor solutions were prepared in a glovebox so that syringes could be used to alternate injecting the cation/anion shell component to grow the ZnS shell layer by layer. These solutions consisted of 0.05 M zinc formate in oleylamine and 0.1 M hexamethyldisilathiane ($\text{S}(\text{TMS})_2$) in trioctylphosphine. The solutions were kept in vials with stir bars in the glovebox until each injection was needed. The sulfur solution was capped with a septum to contain unpleasant sulfur smell as best as possible. Purified CdSe cores ($0.12 \mu\text{mol}$) with a Φ_{PL} of 16% were added to a 50 mL three-neck flask that contained a stir bar, octadecene (6 mL), oleylamine (6 mL), trioctylphosphine (4 mL), and 1-dodecylphosphonic acid ($40 \mu\text{mol}$). After a condenser, septum, and thermocouple were attached, the flask was evacuated to remove air and hexane for the QD purification. The mixture was degassed with multiple rounds of vacuum/purging with nitrogen and heated to 80°C under vacuum for >1 h and then filled with nitrogen. For the first ZnS layer, Zn-oleylamine ($606 \mu\text{L}$, 0.05 M) was injected into the CdSe core solution over 15 min by a syringe pump at 80°C and heated. After the temperature reached 160°C , $\text{S}(\text{TMS})_2$ ($303 \mu\text{L}$, 0.1 M) was injected over 15 min and allowed to anneal for another 30 min. Φ_{PL} increased to 52%. The second ZnS layer was grown by injecting Zn-oleylamine ($866 \mu\text{L}$, 0.05 M) at 160°C over 15 min and then heated to 180°C where $\text{S}(\text{TMS})_2$ ($433 \mu\text{L}$, 0.1 M) was injected. The ZnS layer was annealed for 30 min. Φ_{PL} was 47%. The third layer of ZnS was grown similarly but used Zn-oleylamine ($1170 \mu\text{L}$, 0.05 M) and $\text{S}(\text{TMS})_2$ ($586 \mu\text{L}$, 0.1 M) at 180°C . Φ_{PL} was 53%. Oleic acid (0.5 mL) was added slowly, and the core/shell QDs were allowed to anneal at 200°C for 1 h.

Synthesis of InPZnS Alloyed Core and InPZnS/ZnS Core/ Shell Quantum Dots from Molecular Precursors (InPZnS MP QDs) and (InPZnS/ZnS MP QDs).

InPZnS MP alloyed core and InPZnS/ZnS MP alloyed core/shell QDs were made according to established literature procedures with minor adjustments.⁴ The phosphorus precursor was prepared in a nitrogen-filled glovebox by dispersing $\text{P}(\text{TMS})_3$ (0.1 mmol) in octadecene (2 mL), drawn into a syringe, capped, and left in the glovebox antechamber until ready for injection. Indium acetate (0.2 mmol), myristic acid (0.86 mmol), and octadecene (16 mL) were loaded into a 50 mL three-neck flask equipped with a stir bar, a condenser, a septum, and a thermocouple. The vessel was degassed by multiple vacuum/purge cycles and heated at 100°C under vacuum for >1.5 h to form indium myristate. The mixture was cooled to room temperature, and zinc stearate (0.2 mmol) and 1-dodecanethiol (0.05 mmol) were added. The mixture was again degassed and heated under vacuum to 50°C , at which point it was put under nitrogen for continued heating. When ready to inject the phosphorus solution, the heating mantle was set to a high setting ($>300^\circ\text{C}$). At 220°C , the $\text{P}(\text{TMS})_3$ solution was

quickly injected. The temperature decreased to 210 °C and increased quickly to 285 °C. The time from injection to reaching 280 °C was about 10 min. Crystal growth was allowed to continue for an additional 10 min (280–285 °C). The reaction was terminated by cooling quickly to room temperature. One milliliter of the InPZnS MP QD cores was removed for characterization and degradation studies. Shelling InPZnS MP cores to form InPZnS/ZnS MP core/shell QDs was performed by adding zinc stearate (0.375 mmol) to the crude room temperature InPZnS MP cores described above without purification. The mixture was degassed and heated under vacuum to 100 °C and backfilled with nitrogen. The flask was kept at 230 °C for 3 h, at which point 1-dodecanethiol (0.75 mmol) in octadecene (2 mL) was slowly injected into the mixture. The ZnS shell was allowed to grow at 230 °C for 1 h. The InPZnS/ZnS MP QDs were stored in a vial away from light. They can be purified similarly to other hydrophobic QDs using hexane, acetone, and centrifugation to selectively disperse, flocculate, and separate insoluble QDs or impurities from soluble ones.

InP MSCs and InPZn QD Characterization.

The optical properties of InP MSCs, InPZn MSC core QD, and InPZn/ZnS MSC core/shell QDs were determined with a Thermo Scientific Evolution 201 UV–vis spectrophotometer (excitonic peak) and a PTI Quantum Master 400 fluorimeter (Φ_{PL} , peak position (λ_{max}) and peak full width at half-maximum (fwhm)). Φ_{PL} was determined using a K-Sphere Petite integrating sphere using a 375 nm excitation wavelength, 1.35 nm excitation slits, and 0.5 nm emission slits. Crude reaction mixtures were diluted in hexane and centrifuged, and the translucent QD supernatant was transferred to a clean vial before optical measurements were performed. Final concentrations were adjusted to less than 0.1 absorbance at excitation λ_{375} before photoluminescence spectra/ Φ_{PL} were measured. Standard deviation is given for each QD batch (Table 2) determined by three purifications and measurements of each crude reaction mixture on three different days.

ICP-MS Measurements of InP(MA) MSCs.

ICP-MS measurements were conducted to determine the precise amounts of In(III) in the MSC batches to calculate the molar extinction coefficient for the MSCs. Different batches of InP(MA) MSCs were used to determine $[In^{3+}]$ in InP MSC samples after acid digestion (see Supporting Information for a detailed example of calculation). InP MSCs were digested in a 70% HNO_3 solution. The digested samples were diluted to solutions with In(III) concentrations between 1 ppb and 1 ppm. We used a molecular formula of $In_{37}P_{20}(O_2H_{17}C_{14})_{51}$ for our myristate-coated InP MSCs. This was based on the molecular formula of PA-coated InP MSC $In_{37}P_{20}$ previously reported by Cossairt and co-workers¹⁹ while accounting for changes in ligand molecular weight. This formula was used to estimate In(III) concentration of these solutions to contain amounts that fell within the ICP-MS instrument's best detection window (1 ppm to 1 ppb). Standard curves were made from diluting indium (1 $\mu g/mL$ indium in 2% HNO_3 PerkinElmer Pure Plus #N9304234) to six concentrations between 1 ppb and 1 ppm in 2% HNO_3 . The digested samples were compared to the standard curve ($R^2 = 0.9938$) to give In(III) content using the In^{114} isotope. All samples and standards were made to 2% HNO_3 concentration and used MS grade reagents.

XPS Analysis of InP MSCs.

InP MSCs were smeared onto a silicon chip and analyzed by X-ray photoelectron spectroscopy (XPS) on a Phi 5600 ($P_{\text{base}} < 5 \times 10^{-9}$ Torr) with a Mg $K\alpha$ X-ray source (1253.6 eV, 15 kV, 300 W); photoelectrons were detected at a pass energy of 58.7 eV with a scan rate of 0.125 eV/step. Casa XPS software was used to calibrate all spectra to the C (1s) to the hydrocarbon group at 248.8 eV, fit each peak with a Tougaard background, and fit the P (2p) peak to calculate atomic percentages.

Degradation Studies.

QD cores (CdSe, InPZnS MP, and InPZn MSC) were stored in a nitrogen-filled glovebox. Core/shell QDs (CdSe/ZnS, InPZnS/ZnS MP, InPZn/ZnS MSC) were stored in a dark drawer at room temperature. InPZn MSC QDs (25% Zn/In) were the QD core used for all stability studies to represent the QD made from magic-sized clusters. One hundred microliters of stock QDs [10–90 μM] was dispersed in 1 mL of toluene and centrifuged at 4000g for 10 min to remove insoluble material leftover from the synthesis. The supernatant was passed through a 0.45 μm nylon syringe filter, rinsed, and diluted with toluene to give absorbance values around 0.03 at the lowest energy excitonic peak (~500–550 nm). Glass cuvettes were selected that gave similar absorbances using a dedicated toluene-filled blank cuvette. All samples were kept in these matched glass cuvettes with a small stir bar and PTFE-lined screw top or a rubber septum top for the duration of the degradation experiment. Samples that are described as being kept in the dark were stored in a drawer at room temperature. All other samples were kept in the hood and exposed to ambient room light and sunlight (both oscillating between day and night). For degradation experiments under nitrogen, nitrogen was bubbled through the QD solution, and slight positive nitrogen pressure was provided through a needle in the septum-capped cuvette during the experiment. For the heated samples, some toluene was lost over the course of the experiment. This solvent level was returned by carefully adding nitrogen-infused or standard benchtop toluene (as appropriate) before each measurement to avoid any absorbance changes due to concentration. Nitrogen was bubbled through the samples for 15 min before being returned to heat anytime the nitrogen samples were removed from the Schlenk line. Before every measurement, the samples were allowed to cool to room temperature.

RESULTS AND DISCUSSION

Characterization of InP MSCs.

Structural and spectroscopic characterization of InP(MA) MSCs is provided in Figure 1. High-resolution transmission electron microscopy (HRTEM) images of InP MSCs are difficult to obtain due to the small size (1–2 nm) and low z contrast between InP MSCs and the carbon film of the TEM grids. Poorly resolved nanoparticles can be seen in HRTEM images (see Supporting Information Figure S1). Significantly higher contrast is obtained by using scanning transmission electron microscopy (STEM), which is equipped with a high-angle annular darkfield (HAADF) imaging detector. Figure 1a shows a representative STEM image of InP(MA) MSCs. A histogram showing the size distribution of the MSCs is shown in the inset (details on instrument and analysis are given in the Supporting Information). The use of STEM enables, for the first time, visual observation and quantitative image analysis,

which reveals that the InP MSCs have an average diameter of 1.3 nm with a standard deviation (SD) = 0.37 nm. The polydispersity in the MSC size is attributed to the low signal/background ratio in STEM images of InP MSCs in this size range and to the asymmetric crystal structure of InP MSCs.¹⁹ UV-vis measurements (Figure 1b) show that the InP(MA) MSCs have a well-defined excitonic peak at 384 nm, with a small shoulder at 420 nm, which was attributed in a previous study to two independent optical transitions as calculated using time-dependent density functional theory calculations.⁶ InP(MA) MSC samples that had been exposed to air will show a poorly defined, broad peak (not shown), indicating chemical/ structural degradation. This oxidative degradation is accompanied by the appearance of a phosphate peak in the XPS data (data not shown). Interestingly, even MSC samples with poorly defined peaks could be used as a single source precursor to yield high-quality InP QDs. This result indicates significant structural rearrangement at the high temperatures used to form InP QDs from InP MSCs versus a purely agglomeration growth mechanism.

XPS Analysis of InP(MA) MSCs.

X-ray photoelectron spectroscopy spectra of InP(MA) MSCs shown in Figure 1c confirm the formation of indium phosphide with an In(3d_{5/2}) binding energy at 444.7 eV, within the average of eight NIST database values of 444.6 ± 0.6 eV.²⁷ The indium 3d_{3/2} and 3d_{5/2} peaks show a typical spin-orbit splitting of 7.5 eV. The lack of additional peaks, asymmetry, or broadening indicates well-passivated indium with no other indium-containing surface species present. In the P(2p) region, the single peak at 128.6 eV is consistent with literature values for InP at 128.6 ± 0.6 eV. The absence of any oxidized phosphorus atoms (binding energy ≈ 135 eV) confirms the effectiveness of ligand passivation toward phosphorus oxidation. The small peak to the low binding energy side of the P(2p) peak is due to an In(4s) transition. XPS spectral analysis of the In(3d_{5/2}) and P(2p), which includes consideration of differences in relative sensitivity factors as well as differences in electron transmission and escape depths, reveals an atomic composition ratio of 72% In/28% P. Within the instrumental error of XPS measurements, this ratio agrees well with the core crystal structure of In₃₇P₂₀ for InP MSCs, which was proposed by Cossairt and co-workers (65:35 In/P ratio) for InP(PA) MSCs.¹⁷ The C(1s) region shows a dominant peak at 284.8 eV due to CH₂/CH₃ carbon atoms with a smaller carboxyl peak at 288.4 eV. The presence of these two features as well as their intensity ratio (14:1 CH/CH:COO⁻ ratio) is consistent with the presence of the myristate ligand (CH₃(CH₂)₁₂COO⁻). Overall, the XPS measurements indicate the formation of pure InP(MA) MSCs.

UV-Vis Spectroscopy of InP MSCs.

A combination of UV-vis and ICP-MS measurements was used to determine the molar absorptivity (ϵ_{384}) of InP(MA) MSCs. The concentrations of InP(MA) MSC samples were determined by utilizing ICP-MS measurements to quantify indium content. Using the previously reported atomic formula of InP MSCs of In₃₇P₂₀,¹⁷ we could accurately determine cluster concentration as mol/gram of dry InP(MA) MSCs. ICP-MS was used to remove any false contributions to the sample weight that may come from incomplete washing of MSCs. As such, dry purified InP(MA) MSCs were carefully weighed and dispersed in hexanes in a volumetric flask to give absorbance values between 0.1 and 1. As

these were the same MSC batches analyzed by ICP-MS, we could therefore calculate InP(MA) MSC molarity. The extinction coefficient is derived from Beer's law, $\epsilon = \frac{A}{cb}$, where A is absorbance, c is concentration, and b is the path length of light (1 cm in our cuvette). We determine the extinction coefficient at the excitonic peak (ϵ_{384}) to be $2.8 \times 10^4 \text{ L mol}^{-1} \text{ cm}^{-1}$ with a relative SD of 4.4%. This absorptivity value agrees with the absorptivity value of $\epsilon_{390 \text{ nm}} = 1.9 \times 10^4 \text{ L mol}^{-1} \text{ cm}^{-1}$ for PA-coated InP(PA) MSCs.¹⁷ Figure 1b describes the wavelength dependence of the extinction coefficient, ϵ , of InP(MA) MSCs on a per particle basis. ϵ_{310} and ϵ_{350} on a per InP unit basis are often used to determine InP concentrations, and because these values are often size-independent, absorption at these wavelengths scales predictably with particle volume and the number of InP units in a particle. Talapin and Bawendi have provided ϵ_{310} and ϵ_{350} per InP unit of 5135 and 3700 $\text{L mol}^{-1} \text{ cm}^{-1}$, respectively.^{28,29} Looking at ϵ per MSC (from Figure 1b) and dividing by 20 (the number of neutral InP units per MSC), we calculate the per InP unit ϵ_{310} and ϵ_{350} to be 3155 and 1200 $\text{L mol}^{-1} \text{ cm}^{-1}$, respectively. These ϵ (per InP unit) deviate slightly from the ones reported by Talapin and Bawendi but agree quite closely with 3200 and 1300 $\text{L mol}^{-1} \text{ cm}^{-1}$ determined by Cossairt for PA-coated InP MSCs.¹⁹ A few comments on the discrepancies: Both Talapin and Bawendi used fully formed QDs to calculate molar extinction values where the crystal structure is more similar to bulk zinc blende, compared to the altered crystal structure of InP MSCs.¹⁹ It appears that this deviation from bulk crystal structure also affects the extinction coefficient of the clusters by lowering it. Additionally, the absorption value at 350 nm of our MSCs lies within the excitonic feature of the cluster; therefore, it is not size-independent like one would see in larger particles.

InPZn QD Growth from MSCs Monitored Using UV–Vis Photoluminescence and Scanning Transmission Electron Microscopy.

The synthesis of InPZn QDs from InP(MA) MSCs was monitored by STEM imaging to measure changes in QD diameter. STEM images in Figure 2a (zinc/ indium in the reaction mixture of 200%) and Figure 2b (zinc free, i.e., 0%) show that adding zinc stearate to the hot solvent before injection, while keeping all other reaction conditions identical, causes a significant restriction to QD crystal growth. InPZn QDs (zinc/indium ratio of 200% in the reaction mixture) average 2.1 nm in diameter with a standard deviation SD = 0.49 nm (Figure 2a), whereas zinc-free InP QDs average 3.1 nm in diameter with SD = 0.54 nm (Figure 2b). UV–vis spectroscopy (Figure 2c,d) shows a red shift in the absorption peak as the QDs grow, consistent with quantum-confined excitons. The zinc-free 3.1 nm InP QDs have an absorption maximum at 553 nm (2.24 eV) (Figure 2d). This result is in excellent agreement with previous studies by Micic et al. and Talapin et al., who reported energy band gaps of 2.2 and 2.19 eV for 3 nm InP QDs.^{28,30} The InPZn QDs (Figure 2c) have an absorption peak at 455 nm. For the InPZn/ZnS QDs prepared from InP(MA) MSCs, a plot describing the emission peak position in energy units (eV) of InPZn QDs versus the indium/zinc ratio in the reaction mixture is shown in Figure S2. An inflection point at a zinc/indium ratio of 25% is observed. This could be attributed to a combination of two mechanisms that affect the emission peak wavelength of InPZn QDs. The blue shift of the InPZn QDs with increasing zinc/ indium ratio in the reaction mixture used to form the InPZn QDs from InP MSCs is attributed in part to the inclusion of zinc into the InP QDs to possibly form an

InPZn alloy QD and to a steric effect in the presence of zinc stearate, which restricts InPZn QD crystal growth. Regardless of the exact InPZn QD structure, adding zinc stearate to the reaction mixture provides a simple and predictable way to tune the QD size and emission color over a broad spectral range.

Controlling InP QD Size and Emission Peak Wavelength Using Zinc Stearate.

An important discovery in our work is that the inclusion of zinc stearate in the hot injection step produces highly emissive QDs with narrow emission peaks after shelling and provides excellent control over the emission peak wavelength, λ_{max} . The ability to produce luminescent QDs with tunable emission colors is a defining characteristic of luminescent semiconductor QDs. This allows the QD emission color to be tuned for specific applications with strict requirements, such as multiplexed cellular probes, Forster resonance energy transfer probes, and electronic displays.^{19,20} To isolate the effect of zinc stearate, we varied the amount of zinc in the hot reaction mixture over a wide range of concentrations. One hundred milligram InP(MA) MSC (6 μmol MSCs = 225 μmol In³⁺) samples were used in each reaction, whereas the zinc/indium molar ratio was varied between 0 and 200% (0 to 450 μmol zinc stearate). All other reaction conditions including solvent volume and reaction temperature and time were kept the same. The emission spectra of InPZn/ZnS core/shell QDs with varying amounts of zinc in the reaction mixture are shown in Figure 3. Varying the amount of zinc in the reaction mixture from 0 to 200% results in tunable emission peaks of InPZn/ZnS QDs over the blue-green to yellow-orange ends of the visible spectrum. Table 2 shows the emission peak wavelength, λ_{max} (nm), peak full width at half-maximum (fwhm) in wavelength (nm) and energy (eV) units, and emission quantum yield (Φ_{PL}) of the InPZn/ZnS QDs shown in Figure 3. The fwhm and Φ_{PL} change only slightly over this spectral window. The average fwhm of the InPZn/ZnS QDs is 50 nm (2.2 eV) with a relative SD of 3.3%. The average Φ_{PL} of the InPZn/ZnS QDs is 48% with a relative SD of 6%. This is an improvement in InP QD synthesis as most methods to tune the emission peaks of luminescent QDs by varying their size require adjusting multiple reagent concentrations and/or temperature to yield optimal results with respect to emission peak widths and quantum yield. It should be noted that the inclusion of sulfur in the reaction mixture used to form the InP QDs from InP MSCs had a much smaller effect on the QD emission spectra compared to the effect of zinc stearate (data not shown). Only a slight shift in the emission peak was observed when increasing levels of 1-dodecanethiol to realize a sulfur/indium ratio of up to 10% were included in the reaction mixture. Adding larger amounts of sulfur (>10% sulfur/indium) resulted in emission peak broadening. Furthermore, 1-dodecanethiol quickly degraded the excitonic peak of InP-(MA) MSCs at room temperature, indicating that the sulfur ligands destabilize the InP MSCs similarly to the previously reported effect of amines on InP MSCs.^{6,9} This excludes the possibility of adding 1-dodecanethiol directly to the InP(MA) MSC solution prior to injection. It must be added after the formation of InPZn QDs as a shell precursor.

Thermal and Chemical Stability Studies of InPZn Core and InPZn/ZnS Core/Shell QDs.

As described above, forming InPZn/ZnS QDs from InP MSCs results in excellent photophysical properties including high emission quantum yield and narrow, symmetric, and tunable emission peaks. The QDs maintain their optical properties when stored in the dark in

the presence of excess stabilizing ligands. However, any optical nanomaterial offered as a replacement to CdSe QDs should also provide long-term thermal and chemical stability under operating conditions in the absence of excess ligands. We therefore compared the long-term thermal and chemical stability of InPZnS alloy QDs made from molecular precursors ($\text{P}(\text{TMS})_3$ and indium myristate) and InPZn QDs made from MSCs to the thermal and chemical stability of CdSe QDs toward oxidation. Figure 4 shows UV-vis absorption spectra of CdSe and InPZn QDs over 48 h once excess stabilizing ligands are removed. The QDs were suspended in toluene and kept at room temperature in a capped cuvette. No effort was made to exclude oxygen from the QD solution. Figure 4a,d describes the chemical stability of CdSe QDs toward oxidation when stored in room light (Figure 4a) and in the dark (Figure 4d). When stored in room light (Figure 4a), a decrease in the high energy absorption peak of CdSe QDs at 410 nm is observed. However, no significant change in the band edge absorption peak at 520 nm is observed. When stored in the dark, no significant changes in the absorption peaks of CdSe QD are observed (Figure 4c). Figure 4b,e follows the chemical stability of InPZnS QDs made from molecular precursors (InPZn MP QDs) when stored in room light (Figure 4b) and in the dark (Figure 4e). A significant decrease in InPZnS MP QD band edge absorption along with a blue shift are observed over 28 h when the QDs are stored in room light (Figure 4b). The absorption spectrum stabilizes and remains almost constant over longer periods of observation up to 48 h, possibly due to consumption of oxygen in the headspace of the cuvette. The QD degradation is significantly lower when the InPZnS MP QDs are stored in the dark (Figure 4e). Figure 4c,f shows that similar degradation results are obtained for InPZn QDs made from MSCs (InPZn MSC QDs). The UV-vis absorption results clearly show that InPZn-based QDs degrade faster than CdSe QDs regardless of the synthesis technique used to prepare them, particularly in the presence of light. CdSe QD degradation results in a loss of absorption peaks associated with higher energy transitions, around 410 nm. The band edge transition responsible for photoemission remains relatively sharp, blue shifting slightly. In contrast, the InP-based QDs have their band edge peaks broaden over time. These results indicate that InPZn and InPZnS QDs are clearly more sensitive to photo-oxidation than CdSe QDs.

Because luminescent QDs are often used in devices with operating temperatures higher than room temperature, it is also important to evaluate the thermal stability of InP-based QDs at increased temperature. We chose 90 °C as a representative case. The results of the thermal stability measurements of CdSe QDs and InP-based QDs made from MSCs and from molecular precursors at 90 °C are shown in Figure 5a–c for air-containing QD solutions, and Figure 5d–f for nitrogenated (oxygen-free) QD solutions. Figure 5 shows a significantly higher thermal degradation rate of CdSe and InP-based QDs (compared to results shown in Figure 4) when incubated in air-containing solutions at increased temperature. Figure 5a shows that CdSe QDs maintain their sharp excitonic features when incubated in air-containing solution at 90 °C for 1 h. Only a slight blue shift in the absorption peak of CdSe QDs is observed under these conditions. Figure 5b,c shows a higher degradation rate for InP-based QDs made from molecular precursors (Figure 5b) and from MSCs (Figure 5c) under the same conditions. The rapid InP-based QD degradation, which occurs within 1 h of incubation at increased temperature, might be attributed to oxidation of dangling surface phosphide bonds. Figure 5d–f demonstrates the effect of removing oxygen on the QD

degradation rate under conditions of increased temperature. A significant increase in thermal stability is seen for all QD types. It is also interesting to note that a new higher energy excitonic feature emerges (~313 nm) as the InP-based QDs are purged with nitrogen. Adsorbed oxygen seems to affect this peak more strongly. It is fair to conclude, based on these thermal stability experiments, that under ambient conditions, InP-based QDs are significantly less stable toward oxidation than CdSe QDs. The rate of QD oxidation increases with temperature and decreases with the elimination of oxygen for all QD types. In contrast, oxidation of CdSe QDs when incubated for 1 h at increased temperature impacts higher energy excitonic features with minimal impact on the band edge excitonic feature. This results in the preservation of the emission properties of CdSe QDs when exposed to heat in the presence of oxygen.

Growing a higher band gap material over the QD cores has been used effectively to passivate the QD cores to maximize their photoluminescence and protect the QDs from chemical degradation due to interaction with oxygen and other molecules in their storage solutions. InP-based QDs were coated with ZnS using zinc stearate and 1-dodecanethiol. This method was chosen because it represents the most commonly reported one in the literature and is described in the Materials and Methods section. Figure 6 describes the impact of coating CdSe and InP-based QDs with a ZnS shell on their UV-vis and luminescence properties. Figure 6a–c shows that coating CdSe QDs (Figure 6a) and InPZnS QDs made from molecular precursors (Figure 6b) and InPZn QDs made from MSCs (Figure 6c) significantly decreases the degradation rate of all QD types when suspended in air-containing solutions at room temperature. The excitonic features of CdSe QDs remain highly stable for 14 days under these conditions. Some reduction in QD absorption is observed for InP-based QDs (Figure 6b,c), but their excitonic features are largely preserved regardless of whether they are prepared from molecular precursors or MSCs. Monitoring the photoluminescence spectra of the same samples shows a slight decrease in photoluminescence of CdSe/ZnS QDs during the first day of storage, probably due to the release of loosely bound surface atoms to the solution. As seen in Figure 6d, the CdSe/ZnS photoluminescence remains stable for 14 days after the initial loss of photoluminescence. In contrast, a much larger loss of about 80% in the photoluminescence of the InPZnS/ZnS made from molecular precursors (Figure 6e) and InPZn/ZnS QDs made from InP MSCs (Figure 6f) are observed during the first day. This is while their UV-vis spectra remain largely unchanged. This significant reduction in QD photoluminescence is attributed to poor quality of the ZnS shell as it grows on the III–V QD cores compared to the high quality of the ZnS shell of II–VI CdSe/ZnS QDs. The alloying approach is proposed to overcome poor passivation of core defects with the ZnS shell, which it does in terms of increasing photoluminescence in pristine samples. Once diluted in working concentrations, however, it seems that simply alloying with zinc and sulfur is not sufficient to provide QDs that are structurally stable as the CdSe/ZnS core/shell QDs. Additionally, zinc stearate and 1-dodecanethiol seem to be poor choices for shelling precursors. More reactive sulfur precursors, such as TOP-S, would be a better choice.

SUMMARY

We demonstrated a synthesis route for the formation of highly luminescent InPZn/ZnS QDs with good optical properties. The synthesis of InPZn/ZnS QDs from InP MSCs can be accomplished in a few hours with no exposure to toxic, pyrophoric reagents. This removes a major obstacle for using luminescent InP QDs as an alternative to cadmium-containing luminescent QDs, such as CdSe QDs in a broad range of applications. Although the spectroscopic properties of InP and InPZn/ZnS QDs are promising, chemical degradation measurements reveal that InP QDs exhibit lower stability toward oxidation than CdSe QDs under conditions of increased temperature in the presence of oxygen. The use of InP MSCs as a single source reactant, which greatly simplifies the synthesis of InP QDs, does not impact their susceptibility to oxidation. As expected, coating InP QDs with a higher band gap energy ZnS shell slows the thermal degradation of InP QDs considerably. However, InPZn/ZnS QDs do not maintain their luminescence properties once excess ligands used to stabilize the QDs are removed. This effect is accelerated when the QDs are exposed to light, heat, and oxygen. This might not prove problematic in applications, such as QD-polymer film composites, where the presence of oxygen could be minimized or even eliminated. However, further advances in shelling procedures are required to enable the formation of stable InP-based core-shell QDs, which are suitable for applications in air-containing solutions at room temperature and under conditions of increased temperature.

Supplementary Material

Refer to Web version on PubMed Central for supplementary material.

ACKNOWLEDGMENTS

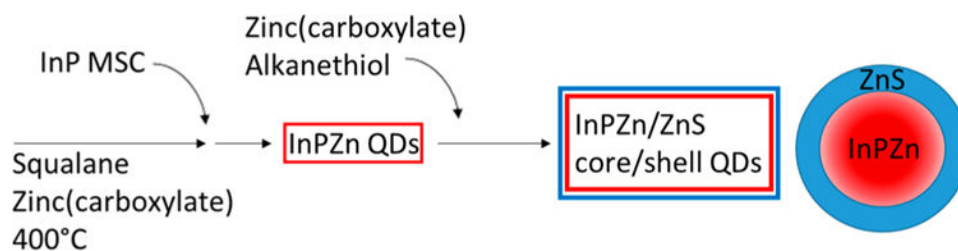
This work was supported primarily by the National Science Foundation Center for Chemical Innovation (CCI) program Award CHE-1503408 for the Center for Sustainable Nano-technology. High-resolution electron microscopy studies of InP MSCs and InPZn/ZnS QDs were supported by NSF Award CHE-1506995. A supplemental fellowship support for R.B.'s graduate assistantship was provided by the UMBC Chemistry Biology Interface program, which is supported by an NIH Training Grant NIH-T32-GM066706. The authors thank Dr. Alline Myers of the NIST Center for Nanoscale Science and Technology for her assistance with TEM imaging.

REFERENCES

- (1). Li L; Reiss P One-pot synthesis of highly luminescent InP/ZnS nanocrystals without precursor injection. *J. Am. Chem. Soc* 2008, 130 (35), 11588. [PubMed: 18686956]
- (2). Kim T; Kim S; Kang M; Kim S-W Large-Scale Synthesis of InPZnS Alloy Quantum Dots with Dodecanethiol as a Composition Controller. *J. Phys. Chem. Lett* 2012, 3 (2), 214–218.
- (3). Xi L; Cho DY; Duchamp M; Boothroyd CB; Lek JY; Besmehn A; Waser R; Lam YM; Kardynal B Understanding the role of single molecular ZnS precursors in the synthesis of In(Zn)P/ ZnS nanocrystals. *ACS Appl. Mater. Interfaces* 2014, 6 (20), 18233–42. [PubMed: 25252171]
- (4). Altintas Y; Talpur M; Unlu M; Mutlugun E Highly Efficient Cd-Free Alloyed Core/Shell Quantum Dots with Optimized Precursor Concentrations. *J. Phys. Chem. C* 2016, 120 (14), 7885–7892.
- (5). Mordvinova NE; Vinokurov AA; Lebedev OI; Kuznetsova TA; Dorofeev SG Addition of Zn during the phosphine-based synthesis of indium phosphide quantum dots: doping and surface passivation. *Beilstein J. Nanotechnol* 2015, 6, 1237–46. [PubMed: 26114082]
- (6). Gary D; Terban M; Billinge S; Cossairt B Two-Step Nucleation and Growth of InP Quantum Dots via Magic-Sized Cluster Intermediates. *Chem. Mater* 2015, 27 (4), 1432–1441.

- (7). Adam S; Talapin D; Borchert H; Lobo A; McGinley C; de Castro A; Haase M; Weller H; Muller T The effect of nanocrystal surface structure on the luminescence properties: Photoemission study of HF-etched InP nanocrystals. *J. Chem. Phys* 2005, 123 (8), 084706. [PubMed: 16164320]
- (8). Haubold S; Haase M; Kornowski A; Weller H Strongly luminescent InP/ZnS core-shell nanoparticles. *ChemPhysChem* 2001, 2 (5), 331–334. [PubMed: 23696509]
- (9). Xie R; Battaglia D; Peng X Colloidal InP nanocrystals as efficient emitters covering blue to near-infrared. *J. Am. Chem. Soc* 2007, 129 (50), 15432–3. [PubMed: 18034486]
- (10). Xu S; Ziegler J; Nann T Rapid synthesis of highly luminescent InP and InP/ZnS nanocrystals. *J. Mater. Chem* 2008, 18 (23), 2653–2656.
- (11). Harris DK; Bawendi MG Improved precursor chemistry for the synthesis of III-V quantum dots. *J. Am. Chem. Soc* 2012, 134 (50), 20211–3. [PubMed: 23228014]
- (12). Gary D; Glassy B; Cossairt B Investigation of Indium Phosphide Quantum Dot Nucleation and Growth Utilizing Triarylsilylphosphine Precursors. *Chem. Mater* 2014, 26 (4), 1734–1744.
- (13). Tessier M; Dupont D; De Nolf K; De Roo J; Hens Z Economic and Size-Tunable Synthesis of InP/ZnE (E = S, Se) Colloidal Quantum Dots. *Chem. Mater* 2015, 27 (13), 4893–4898.
- (14). Pietra F; De Trizio L; Hoekstra AW; Renaud N; Prato M; Grozema FC; Baesjou PJ; Koole R; Manna L; Houtepen AJ Tuning the Lattice Parameter of In_xZn_yP for Highly Luminescent Lattice-Matched Core/Shell Quantum Dots. *ACS Nano* 2016, 10, 4754–4762. [PubMed: 27065247]
- (15). Ramasamy P; Ko K-J; Kang J-W; Lee J-S Two-Step “Seed-Mediated” Synthetic Approach to Colloidal Indium Phosphide Quantum Dots with High-Purity Photo- and Electroluminescence. *Chem. Mater* 2018, 30, 3643–3647.
- (16). Wang Y; Liu YH; Zhang Y; Wang F; Kowalski PJ; Rohrs HW; Loomis RA; Gross ML; Buhro WE Isolation of the magic-size CdSe nanoclusters [(CdSe)₁₃(n-octylamine)₁₃] and [(CdSe)₁₃(oleylamine)₁₃]. *Angew. Chem., Int. Ed* 2012, 51 (25), 6154–7.
- (17). Xie R; Li Z; Peng X Nucleation Kinetics vs Chemical Kinetics in the Initial Formation of Semiconductor Nanocrystals. *J. Am. Chem. Soc* 2009, 131 (42), 15457–15466. [PubMed: 19775131]
- (18). Friedfeld M; Stein J; Cossairt B Main-Group-Semi-conductor Cluster Molecules as Synthetic Intermediates to Nano-structures. *Inorg. Chem* 2017, 56 (15), 8689–8697. [PubMed: 28276683]
- (19). Gary D; Flowers S; Kaminsky W; Petrone A; Li X; Cossairt B Single-Crystal and Electronic Structure of a 1.3 nm Indium Phosphide Nanocluster. *J. Am. Chem. Soc* 2016, 138 (5), 1510–1513. [PubMed: 26784649]
- (20). Jang E; Jo J; Kim M; Yoon S; Lim S; Kim J; Yang H Near-complete photoluminescence retention and improved stability of InP quantum dots after silica embedding for their application to on-chip-packaged light-emitting diodes. *RSC Adv* 2018, 8 (18), 10057–10063.
- (21). Cho S; Kwag J; Jeong S; Baek Y; Kim S Highly Fluorescent and Stable Quantum Dot-Polymer-Layered Double Hydroxide Composites. *Chem. Mater* 2013, 25, 1071–1077.
- (22). Ramasamy P; Kim N; Kang Y; Ramirez O; Lee J Tunable, Bright, and Narrow-Band Luminescence from Colloidal Indium Phosphide Quantum Dots. *Chem. Mater* 2017, 29 (16), 6893–6899.
- (23). Lim J; Bae W; Lee D; Nam M; Jung J; Lee C; Char K; Lee S InP@ZnSeS, Core@Composition Gradient Shell Quantum Dots with Enhanced Stability. *Chem. Mater* 2011, 23 (20), 4459–4463.
- (24). Pietra F; Kirkwood N; De Trizio L; Hoekstra A; Kleibergen L; Renaud N; Koole R; Baesjou P; Manna L; Houtepen A Ga for Zn Cation Exchange Allows for Highly Luminescent and Photostable InZnP-Based Quantum Dots. *Chem. Mater* 2017, 29 (12), 5192–5199. [PubMed: 28706347]
- (25). Zhang J; Li R; Sun W; Wang Q; Miao X; Zhang D Temporal evolutions of the photoluminescence quantum yields of colloidal InP, InAs and their core/shell nanocrystals. *J. Mater. Chem. C* 2014, 2 (22), 4442.
- (26). Jasieniak J; Smith L; van Embden J; Mulvaney P; Califano M Re-examination of the Size-Dependent Absorption Properties of CdSe Quantum Dots. *J. Phys. Chem. C* 2009, 113 (45), 19468–19474.

- (27). NIST X-ray Photoelectron Spectroscopy Database, version 4.1; National Institute of Standards and Technology: Gaithersburg, MD, 2012.
- (28). Talapin DV Experimental and theoretical studies on the formation of highly luminescent II–VI, III–V and core–shell semiconductor nanocrystals Ph.D. Thesis, University of Hamburg, 2002; pp 1–149.
- (29). Xie L; Shen Y; Franke D; Sebastian V; Bawendi M; Jensen K Characterization of Indium Phosphide Quantum Dot Growth Intermediates Using MALDI-TOF Mass Spectrometry. J. Am. Chem. Soc 2016, 138 (41), 13469–13472. [PubMed: 27690411]
- (30). Micic O; Cheong H; Fu H; Zunger A; Sprague J; Mascarenhas A; Nozik A Size-dependent spectroscopy of InP quantum dots. J. Phys. Chem. B 1997, 101 (25), 4904–4912.

**Scheme 1.**

Synthesis of InPZn and InPZn/ZnS Quantum Dots from InP Magic-Sized Clusters

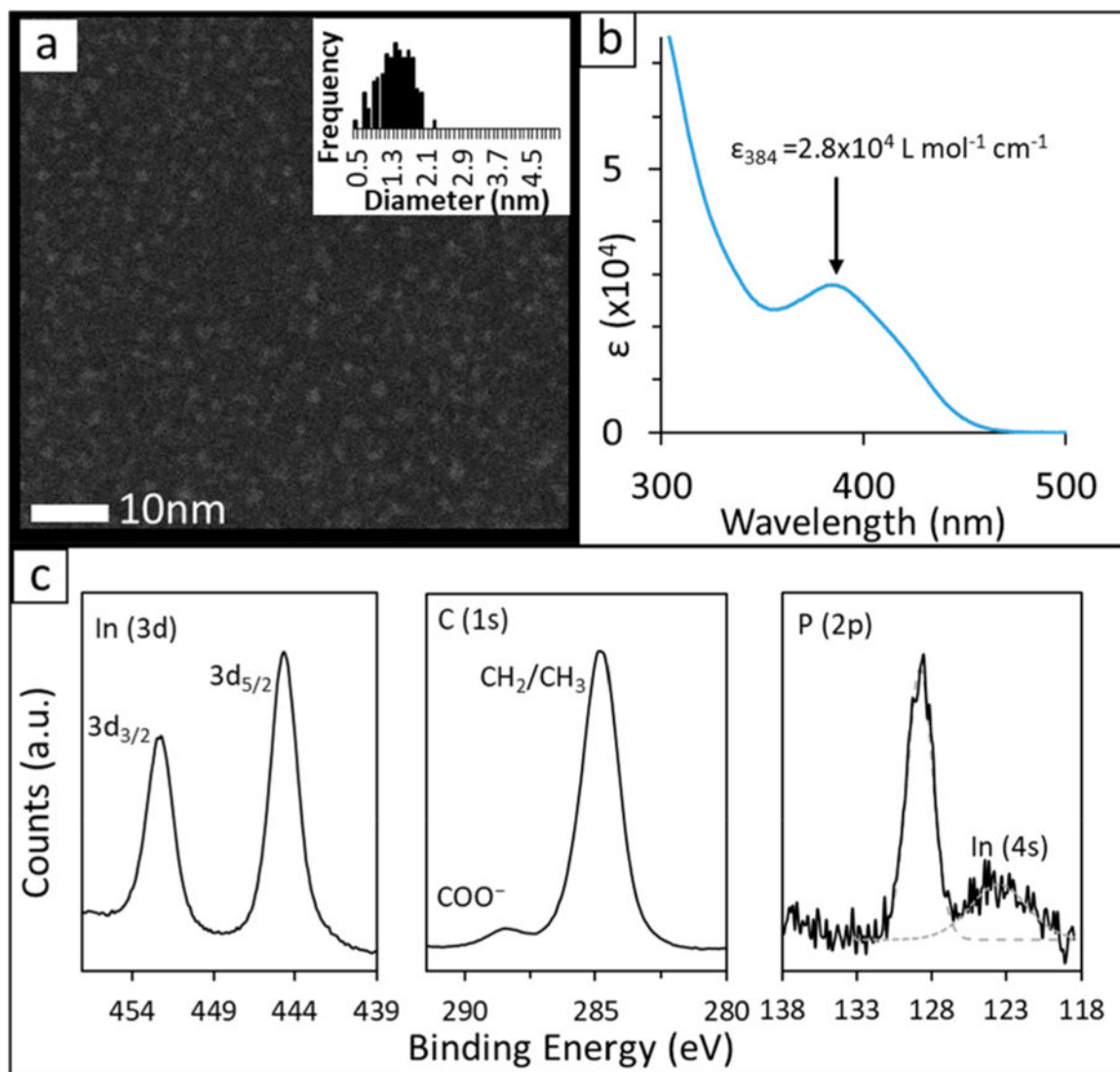


Figure 1.

(a) STEM image of InP(MA) MSCs. The size distribution histogram (inset) reveals an average MSC diameter of 1.3 nm with a standard deviation of 0.37 nm based on the analysis of $n > 200$ MSCs. (b) Absolute UV-vis absorption spectrum of $6.6 \mu\text{M}$ InP(MA) MSC solution showing a well-defined excitonic peak at 384 nm and a shoulder at 420 nm. Extinction coefficient is given on the y -axis. (c) XPS measurements of InP MSCs confirm the presence of indium and phosphorus and agree with the previously reported atomic formula of InP MSCs ($\text{In}_{37}\text{P}_{20}$).

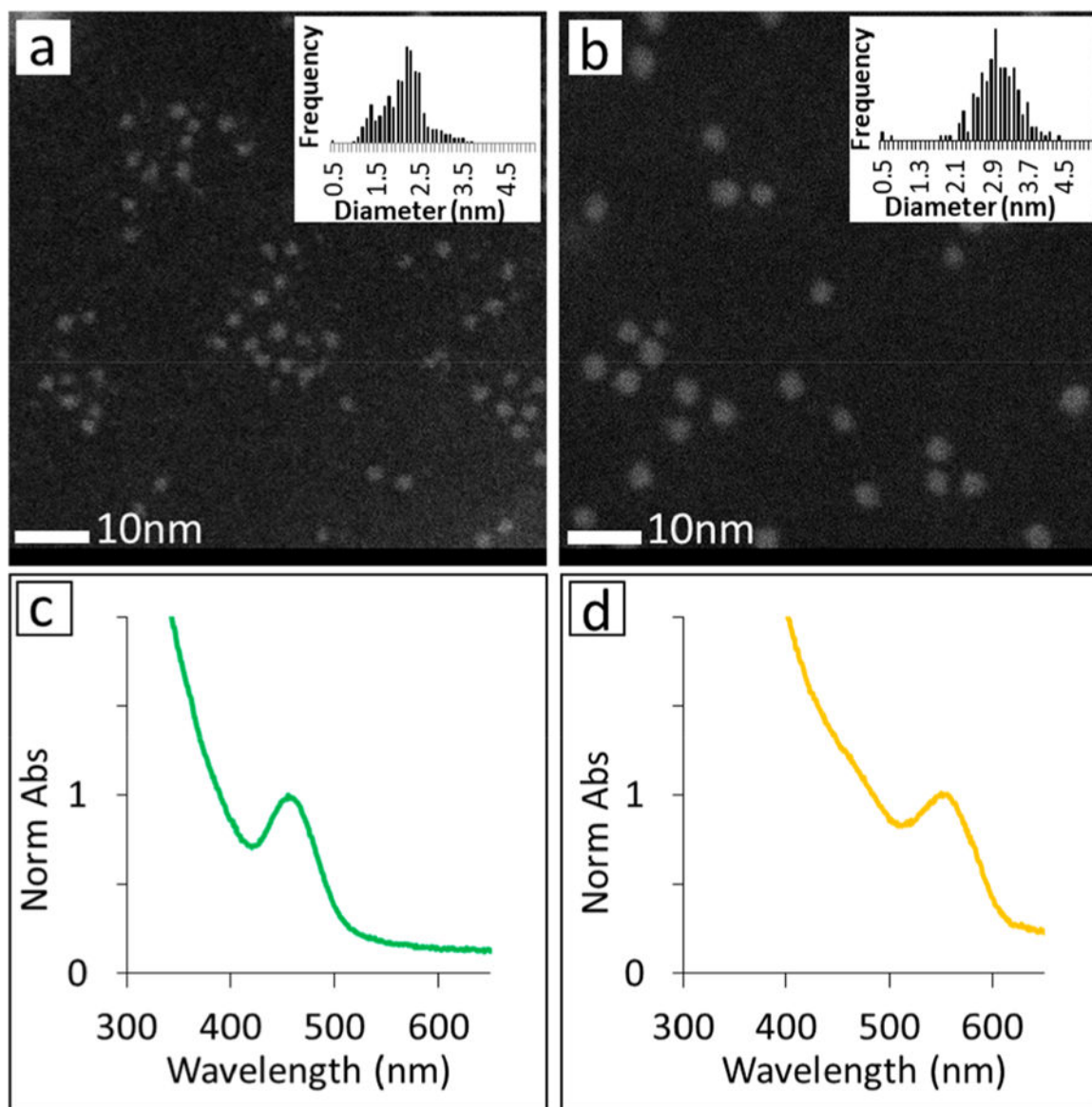


Figure 2.

(a,b) STEM images of InPZn QDs (zinc/indium ratio of 200% in the reaction mixture) and InP QDs (zinc-free reaction mixture). Histograms showing the size distributions of the resulting QDs are shown in insets. (c,d) UV-vis spectra of InPZn QDs (zinc/ indium ratio of 200% in the reaction mixture) and InP QDs (zinc-free reaction mixture). The STEM images and UV-vis spectra show that adding zinc stearate to the reaction mixture used to form InP QDs from InP MSCs leads to the formation of zinc-containing InPZn QDs, which are smaller and have a shorter excitonic peak wavelength than zinc-free InP QDs.

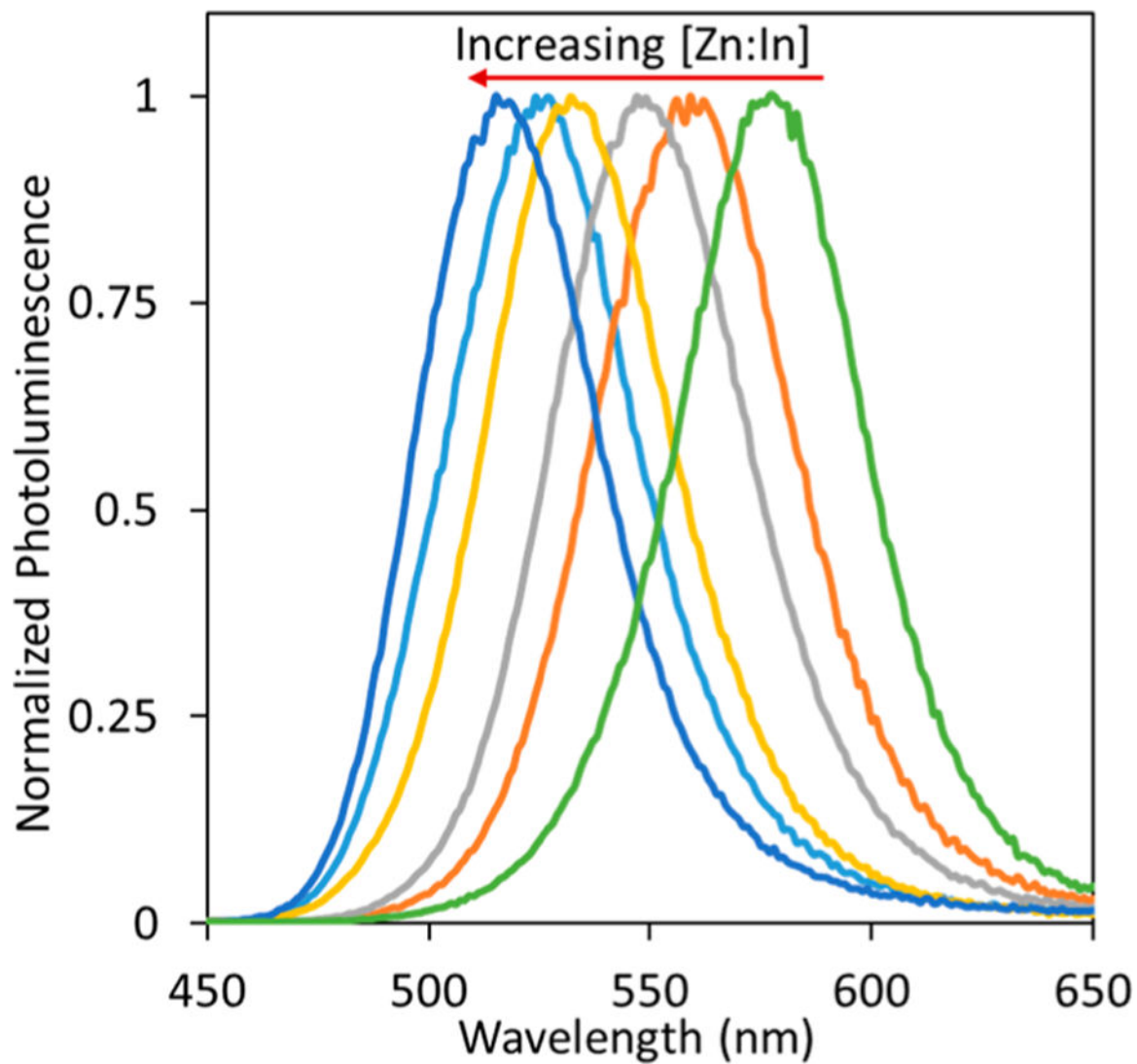


Figure 3. Normalized photoluminescence spectra of InPZn/ZnS core/shell QDs with various zinc/indium ratios in the reaction mixture. From left to right, zinc equals 200, 100, 50, 25, 10, and 0%. Narrow and tunable emission peaks are observed between 500 and 600 nm.

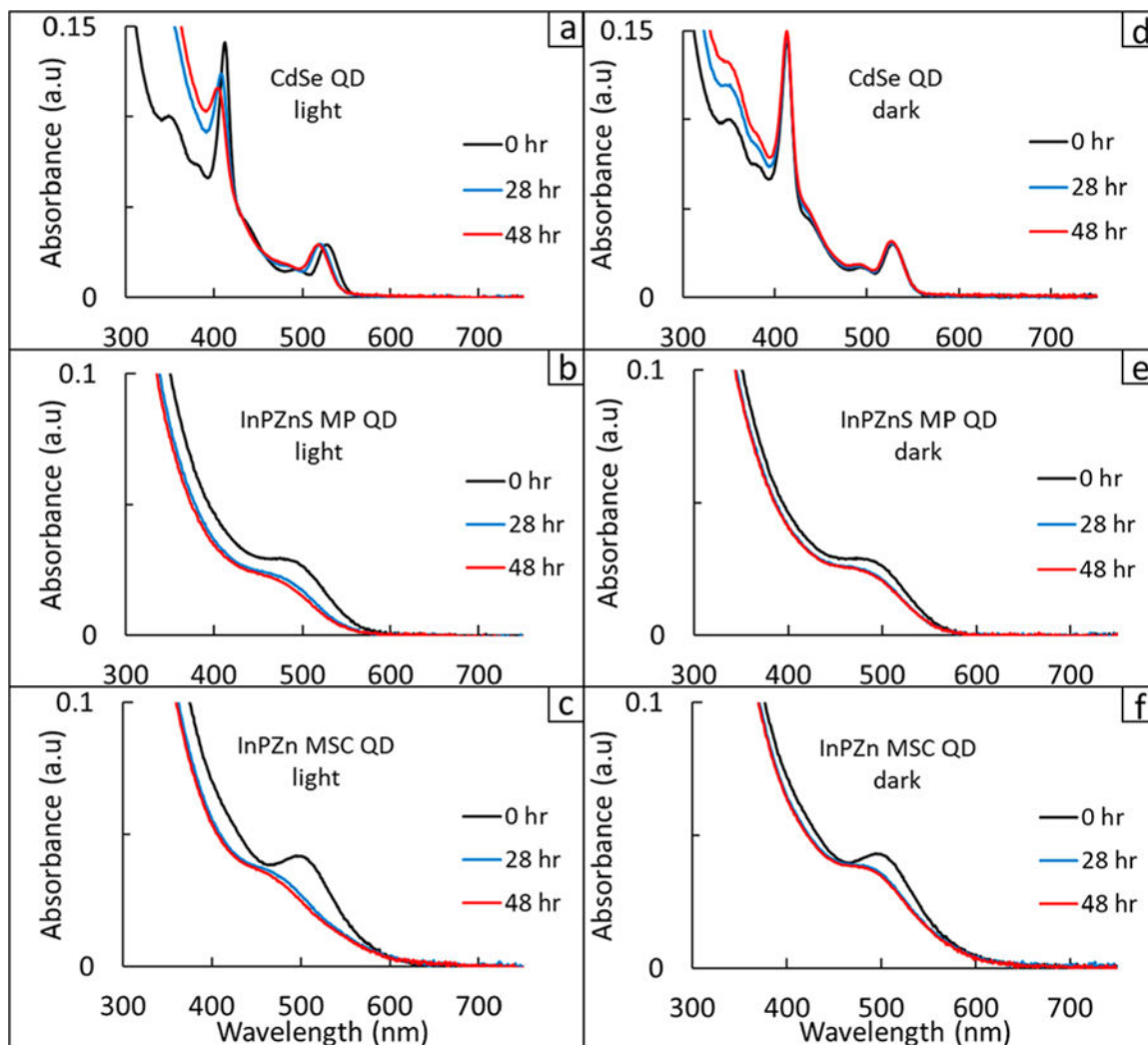


Figure 4.

Degradation of QDs at room temperature when exposed to light (a–c) and when kept in the dark (d–f).

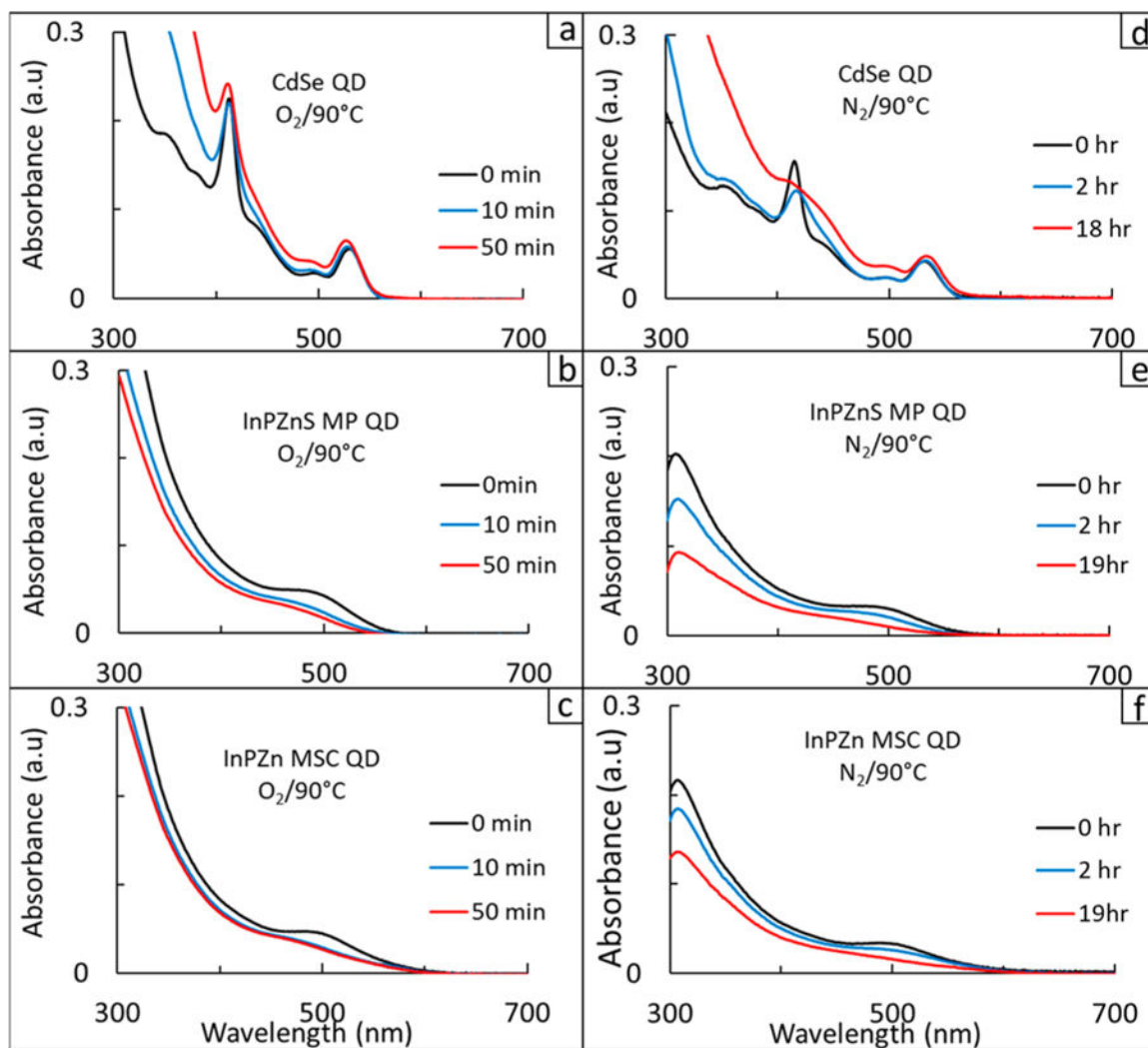


Figure 5.

Degradation of QD cores at 90 °C monitored by UV-vis absorbance: with air (a–c) and under nitrogen (d–f). Please note the different time scales for O_2 versus N_2 conditions.

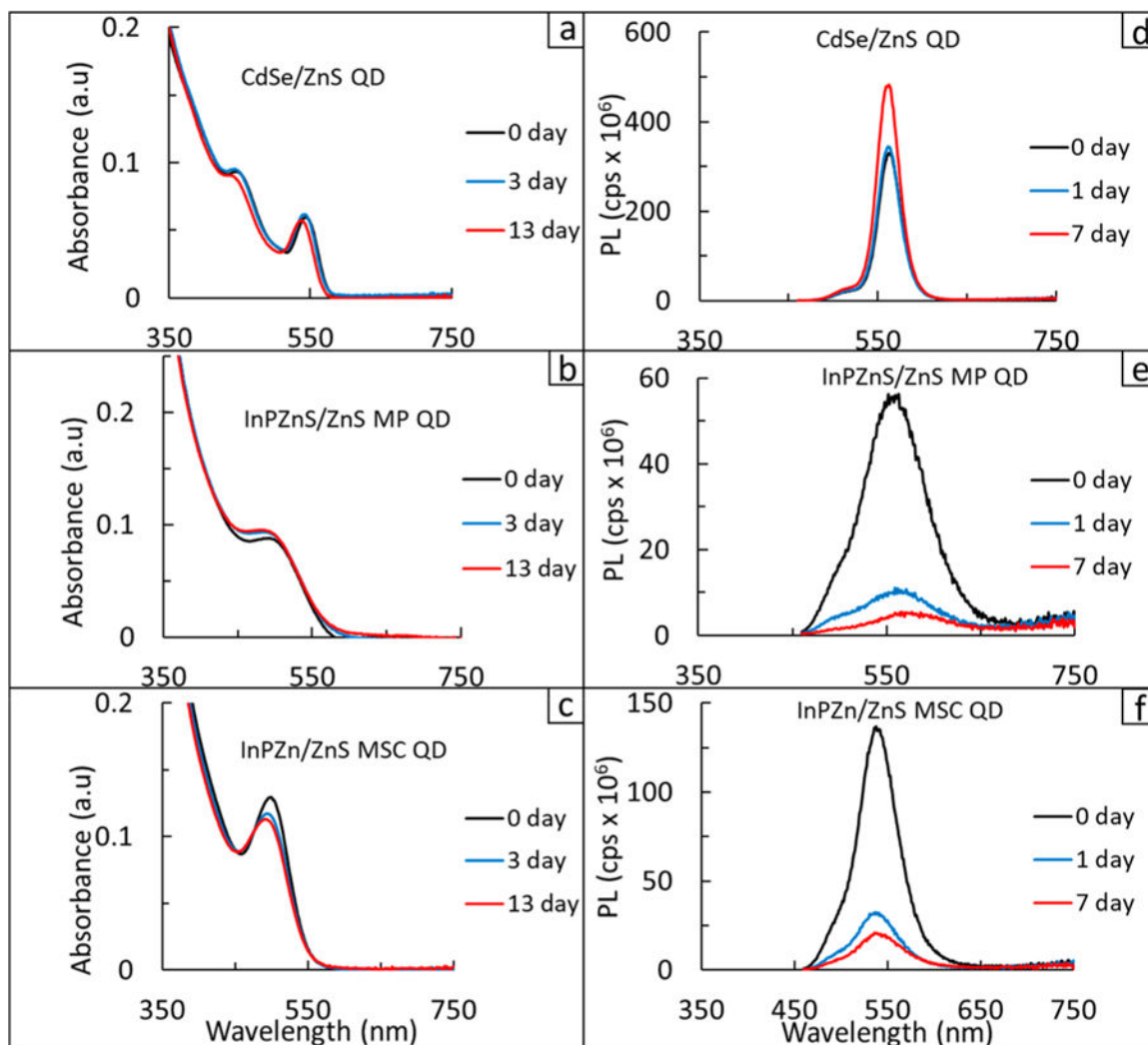


Figure 6.

Degradation of core/shell QDs at room temperature followed by UV-vis (a-c) and photoluminescence (d-f).

Table 1.

Emission Peak Widths from a Selection of Recent InP/ZnS QD Publications Given as Full Width at Half-Maximum^a

reference	~500 nm	~525 nm	~550 nm	~575 nm	~600 nm
Mutlugun (2016)	47 nm	45 nm	67 nm	94 nm	90 nm
Houtepen (2016)	X	X	69 nm	79 nm	70 nm
Reiss (2008)	40 nm	42 nm	50 nm	56 nm	58 nm
this study (2018)	47 nm	50 nm	52 nm	50 nm	X
Lee (2018)	X	37 nm	36 nm	36 nm	37 nm

^aThe values are categorized at the peak's λ_{max} within 25 nm of the λ given in the top row. X indicates that this wavelength was not provided in the original experimenter's data set.

Table 2.

Properties of InPZn/ZnS QDs for Different Zinc/Indium Ratios in the Reaction Mixture: Photoluminescence Peak Wavelength, Emission Peak Full Width at Half-Maximum in Wavelength (λ) and Energy Units (eV), and Photoluminescence Quantum Yield, Φ_{PL}

Zn/In (%)	PL λ_{max} (nm)	fwhm (λ , nm)	fwhm (eV)	Φ_{PL} (%)
200	515	47	0.217	47 ± 3
100	524	50	0.225	49 ± 3
50	532	50	0.218	46 ± 1
25	547	52	0.214	52 ± 2
10	559	52	0.206	47 ± 3
0	577	50	0.187	45 ± 4